Two pairs of ON and OFF retinal ganglion cells are defined by intersectional patterns of transcription factor expression

David L. Rousso[1], **Mu Qiao**[1], **Ruth D. Kagan**[1], **Masahito Yamagata**[1], **Richard D. Palmiter**[2], and **Joshua R. Sanes**[1]

[1]Center for Brain Science and Department of Molecular and Cell Biology, Harvard University, 52 Oxford Street, Cambridge, MA 02138

[2]HHMI and Department of Biochemistry, University of Washington, Seattle, WA

Summary

Visual information is conveyed to the brain by axons of >30 retinal ganglion cell (RGC) types. Characterization of these types is a prerequisite to visual perception understanding. Here we identify a family of RGCs that we call F-RGCs based on expression of the transcription factor *Foxp2*. Intersectional expression of Foxp1 and Brn3 transcription factors divides F-RGCs into four types, comprising two pairs, each composed of closely related cells. One pair, F-mini^{ON} and F-mini^{OFF}, shows robust direction selectivity. They are among the smallest RGCs in the mouse retina. The other pair, F-midi^{ON} and F-midi^{OFF}, are larger and not direction-selective. Together, F-RGCs comprise >20% of RGCs in the mouse retina, halving the number that remain to be classified and doubling the number of known direction-selective cells. Co-expression of Foxp and Brn3 genes also marks subsets of RGCs in macaques that could be primate homologues of F-RGCs.

Graphical abstract

Introduction

The vertebrate retina contains five neuronal classes: photoreceptors, that transduce light into electrical signals, interneurons (bipolar, horizontal, and amacrine cells) that process the information, and retinal ganglion cells (RGCs), that transmit it to the rest of the brain through the optic nerve (Figure 1A) (Masland, 2012; Sanes and Zipursky, 2010). Each class is divided into multiple types, enabling the complex computations that results in different RGCs being tuned to distinct visual features such as contrast, color, or motion in a specific direction (Berson, 2008; Sanes and Masland, 2015). A full accounting of the types of RGCs and their functional properties is therefore prerequisite to understanding how the visual system works.

Initial classification schemes for RGCs in mice were based on their morphological properties (Badea and Nathans, 2004; Coombs et al., 2007; Kong et al., 2005; Sun et al., 2002; Völgyi et al., 2009), leading to identification of approximately 20 RGC types. Recently these methods have been supplemented by molecular, genetic, and functional approaches (Badea and Nathans, 2011; Baden et al., 2016; Dhande and Huberman, 2014; Huberman et al., 2008; Kim et al., 2008; Tien et al., 2015), increasing the estimated number of RGC types to >30. Nonetheless, the total number is unclear and nearly half of all RGCs in mice remain unknown or unclassified (Sanes and Masland, 2015).

To identify novel RGC types, we analyzed combinatorial expression of transcription factors (TFs), a strategy that has been useful for defining cell types in other parts of the CNS (Catela et al., 2015; Lodato and Arlotta, 2015). We screened retinas for expression of ~40 TFs and found that the forkhead/winged-helix domain protein Foxp2 was expressed by 20–25% of RGCs, few if any of which corresponded to previously known types. Combinatorial co-expression of Foxp1 and the Pou4f factors, Brn3a-c, divided Foxp2$^+$ RGCs (F-RGCs) into four discrete types that differ in size, dendritic lamination, and physiological responsiveness.

They comprise a pair of small and abundant direction-selective RGCs, F-mini[ON] and F-mini[OFF], and a pair of larger, less numerous, direction non-selective RGCs, F-midi[ON] and F-midi[OFF]. ("ON" and "OFF" refer to predominant responsiveness to increases and decreases in illumination level, respectively.) F-RGCs comprise more than 20% of RGCs in the mouse retina, halving the number of RGCs that remain to be classified and characterized in mouse, and doubling the number of known direction-selective RGCs.

Our molecular, morphological, and physiological analyses revealed several noteworthy features of F-RGCs. First, F-mini and F-midi RGCs each comprise an ON and OFF pair. Their relationship is reminiscent to the paramorphic pairs described in other species, which are defined as "neuronal cell types differing from one another mainly at the level of dendritic stratification but otherwise more similar to one another than to other types" (Berson, 2008). Paramorphism is a common feature of RGCs in many species (Berson, 2008; Famiglietti, 2004, 2005; Famiglietti and Kolb, 1976; Isayama et al., 2009) but has not been explored extensively in mice; F-RGCs enable future studies into its developmental origin. Second, the F-mini RGCs are direction-selective. The computation of directional motion by retinal neurons is a topic of intense current interest. Most studies have focused on ON-OFF direction selective RGCs (ooDSGCs), which acquire direction selectivity from starburst amacrine cells (Borst and Helmstaedter, 2015; Vaney et al., 2012). The F-mini RGC dendrites overlap little with those of starburst amacrines; they are therefore unlikely to receive substantial input from them and must compute direction by another mechanism. Finally, F-mini RGCs are among the smallest and most numerous RGC types yet identified in mouse. In these and other respects, they resemble midget RGCs, a paramorphic pair comprising the smallest and most abundant RGCs in primates (Dacey and Packer, 2003; Szmajda et al., 2005). Motivated by this parallel, we analyzed macaque retina, and identified RGC subsets that express combinations of Foxp and Brn3 transcription factors. Foxp2^{+} RGCs in macaque exhibit the unusual distribution reported for midget RGCs, a paramorphic pair comprising the smallest and most abundant RGCs in primates (Silviera et al., 2004; Watanabe and Rodieck, 1989).

Results

Foxp2 is expressed by a group of RGCs distinct from currently known types

To identify novel RGC types we assembled a panel of antibodies to 41 TFs that have been used to classify neurons throughout the brain and spinal cord (Table S1) and analyzed their expression in adult mouse retina. Antibodies that labeled between 10 and 30% of RGCs were studied further. Here, we focus first on Foxp2, which, as documented below, labels >20% of RGCs. Foxp proteins have been shown to define different classes of neurons in the brain and spinal cord (Benito-Gonzalez and Alvarez, 2012; Dasen et al., 2008; Hisaoka et al., 2010; Rousso et al., 2008, 2012) but their expression in retina has not been examined.

In sections of adult retina, Foxp2^{+} cells were localized to the ganglion cell layer (GCL). This layer contains both RGCs and amacrine cells. We surveyed co-expression of Foxp2 with the RNA-binding protein RBPMS, which labels all and only RGCs (Rodriguez et al., 2014). At least 90% of Foxp2^{+} cells were co-labeled with RBPMS; <10% expressed Pax6 or Ap2, which mark amacrine cells (Figure 1B, 1C, and data not shown; Bisgrove and Godbout,

1999; de Melo et al., 2003). Thus >90% of Foxp2$^+$ retinal cells are RGCs; hereafter we refer to them as F-RGCs. The few Foxp2$^+$ cells in the inner nuclear layer were displaced RGCs. We next estimated the fraction of total RGCs that are F-RGCs. Although the distribution of F-RGCs varied across the retina (see below), they reach a maximum density of 840 ± 50 cells/mm^2 in the central/ventral region, accounting for $23 \pm 2\%$ of all RGCs in this region (mean $\pm$ SE) (Figure 1D, 1E; note the comparison of Foxp2 RGC density as a group to other RGC types).

Several RGC types have previously been characterized using molecular markers. We used double-staining to ask which, if any, of these known types include F-RGCs. Remarkably, despite their abundance, F-RGCs were distinct from previously characterized types for which we had markers, including alpha-RGCs, ip-RGCs, ooDSGCs, J-RGCs, and W3B-RGCs (Figure 1F, Table 1, and data not shown; Duan et al., 2015; Hattar et al., 2002; Kay et al., 2011; Kim et al., 2008, 2010; Sanes and Masland, 2015). These results raised the possibility that Foxp2 is expressed by previously undescribed RGC types.

Our initial screen was performed on adult retinas. We subsequently analyzed developing retina and observed selective expression of Foxp2 by a subset of RGCs on embryonic (e) day 15.5, the earliest time examined (Figure S1). Most RGCs are "born" (become post-mitotic) between e10 and e14 (Voinescu et al., 2009). Thus Foxp2 may be useful for analyzing the development of F-RGCs.

Combinatorial expression of transcription factors defines four F-RGC types

We next asked whether F-RGCs include one, a few, or a multitude of RGC types. To this end, we exploited the "mosaic" arrangement characteristic of retinal neurons: neurons of a single type are less likely to be near neighbors than would be expected by chance alone, whereas they are randomly distributed with respect to neurons of other types (Figure 2A, 2B; Kay et al., 2012; Reese, 2012; Rockhill et al., 2000). Analysis of spatial distribution using the density recovery profile (DRP) therefore provides a means of assessing whether a set of labeled neurons comprises a natural cell type (Rodieck, 1991). Moreover, the distribution of a mixture of types is distinguishable from that of a single type, allowing for the estimation of the fraction (f) of an array that constitutes an otherwise homogeneous population (f < 1, partial array; f > 1, mixed arrays; Figure 2B; see Supplemental Experimental Procedures for details) (Rodieck, 1991; Zhang et al., 2012). Thus, a mixture of two neuronal types of equal abundance generates an array of f = 2 (Figure 2B). Non-integral numbers suggest the existence of types that differ in abundance. Following this logic, we analyzed the spatial distribution of F-RGCs and found that they deviated significantly from that of a random distribution, with f = 2.2 (Figure 2C, 2D), consistent with the idea that F-RGCs comprise 2 regularly arranged types of similar abundance, plus one or more additional sparse types.

We reexamined TFs from the initial screen to seek intersectional expression patterns that would divide F-RGCs into discrete types. A related protein, Foxp1, divided F-RGCs into two groups whose spatial distributions more closely resembled single arrays yet appeared to contain more than one type each (f > 1) (Figure 2E, 2F); this suggests each group contains 1 abundant and at least 1 sparse type. Consistent with this idea, Pou4f/Brn3 proteins further

divided each of these two groups into one abundant and one sparse type (abundant, Foxp1$^+$/Foxp2$^+$/Brn3b$^-$; sparse, Foxp1$^+$/Foxp2$^+$/Brn3b$^+$; abundant, Foxp1$^-$/Foxp2$^+$/Brn3c$^-$; and sparse, Foxp1$^-$/Foxp2$^+$/Brn3c$^+$) (Figure 2G–2J). Although a range of staining levels was observable for each marker, only the brightest labeled cells were included within each type. DRP and nearest-neighbor spatial analysis confirmed that each type exhibited a region of exclusion surrounding cell bodies of the same type (i.e., A → A), but not to members of another type (i.e., A → B) (Figure 2H, 2J, and S2). Moreover, the exclusion distance of each group was matched by predicted hexagonal arrays of similar side length (f ≈ 1). Thus, Foxp1 and Brn3 proteins divide F-RGCs into 4 molecularly distinct RGC types. The density relationship between the abundant and sparse types for each group was ~4:1.

We simultaneously labeled the four types and tabulated their contribution to the total Foxp2 RGC population (Figure 2K, 2L). Cumulatively they accounted for 87 ± 3 % of all Foxp2$^+$ RGCs (mean ± SE). The remaining cells could not be readily categorized due to dim or ambiguous staining. Thus, the four molecularly defined populations account for most F-RGC types (Figure 2M, 2N).

Correspondence of morphological and molecular distinctions among F-RGCs

To gain genetic access to F-RGCs, we generated animals in which Cre recombinase was inserted at the Foxp2 locus (*Foxp2-Cre*; Figure 3A). When these mice were crossed to reporter lines in which strong expression of a fluorescent protein was Cre-dependent, labeling was widespread, perhaps reflecting broad expression of *Foxp2* during early development. In contrast, when we used an adeno-associated virus (AAV) to deliver a Cre-dependent GFP cassette (*AAV2/9$^{flex-GFP}$*) to mature retina, only Foxp2$^+$ cells were labeled, as judged by co-expression of GFP and Foxp2; we occasionally observed some GFP$^+$ cells that were not Foxp2$^+$, but these were rare (<5%) (Figure 3B). We used sparse labeling with AAV to characterize F-RGCs morphologically.

Each of the four molecularly identified F-RGC types exhibited a stereotyped morphology (Figure 3C–3F). Dendrites of two types stratified in the outer portion of the IPL (~S1 of 5 strata) indicating they were likely to be OFF cells (Famiglietti and Kolb, 1976), a presumption confirmed below. Dendrites of the other two types stratified broadly in the middle portion of the IPL (~S3), suggesting that they were ON or ON-OFF cells (Figure 3G). In each pair, dendritic arbors of one were considerably larger than the other. These characteristics led us to name the cell types F-mini^{OFF} (Foxp1$^+$/Brn3b$^-$), F-midi^{OFF} (Foxp1$^+$/Brn3b$^+$), F-mini^{ON} (Foxp1$^-$/Brn3c$^-$) and F-midi^{ON} (Foxp1$^-$/Brn3c$^+$).

F-mini RGCs were exceptionally small, with dendritic field areas of 8–15,000 μm^2 in central retina, making them as small if not smaller than W3B RGCs, the smallest RGCs previously described (Figure 3H) (Kim et al., 2010; Krishnaswamy et al., 2015; Zhang et al., 2012). F-midi RGCs covered larger dendritic territories than F-mini cells but were nevertheless smaller than several other RGC types, including J-RGCs and alpha-RGCs (Figure 3H).

Remarkably, all four F-RGC types exhibited dendritic asymmetry oriented along the vertical axis (Figure 3I). This asymmetry resembled that of previously described J-RGCs, BD- and HB9-RGCs (Kim et al., 2008; Kay et al., 2011; Trenholm et al., 2011). Although the OFF-F-

RGCs are smaller than J-RGCs, their dendritic asymmetry and lamination patterns are similar (Figure S3).

A hallmark of most RGC types characterized to date is that their dendrites cover the retinal surface at least once, allowing them to report on a visual feature over the entire visual field. Thus, the coverage factor for RGC types, defined as the product of dendritic field area and density (spatial frequency) is   1. Consistent with this idea, F-mini RGCs have a coverage factor of ~2–3X. F-midi RGCs have a lower density but also a larger dendritic area, resulting in a coverage factor of ~1–2X (Figure 3J). These results support the idea that all four F-RGC groups comprise authentic RGC types.

Molecular characterization of F-RGCs

We screened transgenic lines that label characterized RGC types with markers for F-RGCs. For Cre-expressing lines, we used a Cre-dependent reporter, *Thy1-stop-YFP* (Buffelli et al., 2003). Few, if any, F-RGCs were labeled in lines *Cdh3^{GFP}* (includes a set of ip-RGCs; Osterhout et al., 2011); *Cdh6^{CreER}* (includes a set of ooDSGCs; Kay et al., 2011, Trenholm et al., 2011), or *Thywy7* (marks a set of alpha-RGCs; Kim et al., 2010), supporting the idea that that F-RGCs do not correspond to previously characterized types. The two types of OFF-F-RGCs were labeled in the *PV^{Cre}* line (Figure S4A); indeed, PV7 cells likely correspond to F-mini^{OFF} RGCs, rather than J-RGCs as previously described (Farrow et al., 2013). We also analyzed two new lines, *Cdh4^{CreER}* and *Cdh13^{CreER}* (see Experimental Procedures). All F-RGCs were labeled in the *Cdh4^{CreER}* line and the F-mini types were labeled in the *Cdh13^{CreER}* line (Figure S4B, S4C), providing insight into recognition molecules that might influence synaptic choices of these cells.

In parallel, we characterized F-RGCs molecularly by triple-immunostaining retinal whole mounts and sections. Molecules identified included ion channels and channel-associated proteins (Kv4.2 and calsenilin), calcium binding proteins (calretinin and parvalbumin), G protein phosphatase Ppp1r17, and additional TFs from our initial screen (Table 1 and Figure S4D–S4G). All F-RGCs expressed NeuN and Isl2. Within F-RGCs, Isl1 and PV were selectively expressed by the OFF types. Ppp1r17 was expressed by the F-mini^{ON} type, and Satb1, Satb2, and Ebf3 were expressed by the F-midi^{ON} type. These results extend the molecular distinctions among F-RGCs.

F-RGCs project to image-forming brain regions

RGCs project to 20–40 retinorecipient areas in the brain, with distinct RGC types differing in projection patterns (Dhande and Huberman, 2014; Huberman et al., 2009; Kay et al., 2011; Kim et al., 2008; Morin and Studholme, 2014; Osterhout et al., 2011). To identify central targets of F-RGCs we analyzed brains following intravitreal injection of *AAV2/9$^{flex-GFP}$* into *Foxp2^{Cre}* mice. Fluorophore-conjugated cholera toxin B (CTB) was co-injected to label all RGC axons and thus all retinorecipient areas (Figure 4A). F-RGC axons terminated in the dorsal lateral geniculate nucleus (dLGN) and superior colliculus, which are sites in which information about visual features are processed. Within the dLGN, F-RGC axons terminated selectively within the lateral shell (Figure 4B, 4C). Within the colliculus, F-RGC axons stratified broadly within layers 2 and 3 (upper and lower stratum griseum

superficiale; Figure 4D, 4E). In both the thalamus and colliculus, termination fields of F-RGCs are similar to those reported for J-RGCs and ooDSGCs (Huberman et al., 2009; Kay et al., 2011; Kim et al., 2008). In contrast, F-RGC axons largely bypassed the suprachiasmatic nucleus (SCN), to which non-image-forming ip-RGCs project, as well as accessory optic nuclei such as the medial terminal nucleus (MTN) and olivary pretectal nucleus (OPN) (Figure 4F–4I), to which ON-DSGCs and other non-image forming RGCs project. These innervation patterns are consistent with the idea that F-RGCs contribute to visual perception (Figure 4J).

Visual responses of F-RGCs

We labeled F-RGCs in *Foxp2^Cre^* mice, targeted them for recording with pipettes for loose-patch spike recordings, and stimulated them with spots and moving bars of various speeds and direction. Following recording, targeted cells were fixed and cell type was assessed by immunohistochemical criteria. A subset of cells were also marked by dye injection and identified morphologically. Consistent with their relative densities, F-midi cells were encountered ~1/4 as frequently as F-mini cells.

We predicted that there would be two differences among F-RGC types based on their morphological properties. First, RGCs with dendrites that stratify in S1 generally fire when the level of illumination diminishes (OFF response), while RGCs with dendrites in S3 fire either when the level of illumination increases or at both light onset and offset (ON or ON-OFF responses). As expected, F-mini^ON^ RGCs were pure OFF cells and the and F-midi^OFF^ RGCs were predominantly OFF. In contrast, F-mini^ON^ and F-midi^ON^ RGCs were pure ON cells. Responses were transient for three of the four F-RGC types, and were sustained only for F-midi^OFF^ RGCs (Figure 5A–5D).

Second, because the size of the receptive field center of an RGC is generally determined by the size of its dendritic arbor, we expected that F-mini RGCs would have smaller fields than F-midi RGCs. As measured by peak response to light or dark spots of varying sizes, the radii of receptive field centers were ~66 ± 4 μm and ~85 ± 8 μm for F-mini and F-midi RGCs, respectively (mean ± SE; $p < 0.05$) (Figure 5E–5H and 5M). This difference was smaller than expected from their dendritic diameters, but the small number of recordings obtained from F-midi RGCs precluded a robust statistical comparison.

We next examined direction-selectivity using bars moving in each of 8 directions. Examples are shown in Figure 5I–5L and results are summarized in Figure 5N. Both F-mini cell types were direction-selective, with their preferred direction corresponding to the direction in which their dendrites pointed (DSI = 0.33 ± 0.04; mean ± SE) (Figure S5A, S5B). As expected, F-mini^ON^ RGCs fired at the leading edge (onset) of the moving bar, whereas F-mini^OFF^ RGCs responded to the trailing-edge (offset) of motion (Figure S5C, S5D). We tested DS responses over a range of speeds, and found that F-mini cells responded best to bars moving at ~0.5–0.6 mm/s (Figure 5O). This preferred speed is faster than that of ON-DSGCs (~0.25 mm/s) (Yonehara et al., 2009), but slower than that of ooDSGCs (Trenholm et al., 2011). F-midi RGCs were not direction-selective (DSI = 0.09 ± 0.04; mean ± SE) (Figure 5N).

F-RGCs vary in density, size, and orientation along the dorsal-ventral axis

Analysis of whole mount retinas revealed that the density of F-RGCs was graded along the vertical axis: highest in the central/ventral region and lowest in dorsal retina (Figure 6A). We asked whether this feature is shared by all F-RGC types. F-mini[ON] and F-mini[OFF] RGCs were distributed in a ventral-high/dorsal-low gradient, resembling that of F-RGCs in total (Figure 6B, 6C). F-midi[OFF] RGCs were distributed in a steeper gradient; very few cells of this type are found in the dorsal third of the retina (Figure 6D). In contrast, F-midi[ON] RGCs were more numerous in dorsal than in ventral retina (Figure 6E). Thus, all four F-RGC types exhibit anisotropic distributions along the dorso-ventral (DV) axis.

We asked whether non-uniformity in distribution influenced dendritic field coverage of F-RGCs. F-mini[OFF], F-mini[ON], and F-midi[OFF] RGCs, which are denser in ventral retina as compared to dorsal and peripheral regions, were also smaller in ventral retina than in dorsal/peripheral regions. Conversely, F-midi[ON] RGCs were both denser and smaller in dorsal than ventral or peripheral retina (Figure 6F–6I). Thus, dendritic field areas scale with local density, resulting in uniform coverage. Moreover, while fluctuations in density along the DV-axis altered the average spacing between cells, it did not disrupt their overall mosaic architecture (Figure 6J–6M; mean regularity index = 3.44 ± 1.08; regularity/random ratio = 1.78 ± 0.18; Mean ± SE). Thus, F-RGC size, density, and soma distance co-vary proportionately along the DV-axis, maintaining uniform coverage across the retina. These gradients in cell density and dendritic size imply that F-mini[ON], F-mini[OFF], and F-midi[OFF] RGCs all sample the visual world at higher acuity in ventral than dorsal retina, whereas the opposite is true for F-midi[ON] RGCs.

Finally, we assessed the asymmetry of F-RGC dendrites as a function of retinal position. Dendrites of F-mini[OFF], F-midi[OFF], and F-midi[ON] RGCs were predominately ventral-pointing throughout the retina, although we occasionally observed some cells with orthogonal orientations. In striking contrast, the dendritic asymmetry of F-mini[ON] RGC dendrites was position-dependent, pointing ventrally in dorsal retina and dorsally in ventral retina (Figure 6N, 6O, and Figure S6A, S6B). Thus, because the direction of preferred motion for F-mini RGCs corresponded to their dendritic asymmetry, all F-mini[OFF] RGCs preferred ventral motion, whereas for F-mini[ON] RGCs, cells in dorsal retina preferred ventral motion and cells in ventral retina preferred dorsal motion. The dendritic orientation of F-mini[ON] RGCs switched along a horizontal swath ~1 mm above the optic disc, corresponding to the opsin transition zone, in which expression of opsins in cones switches from predominantly short (S) wavelength to middle (M) wavelength opsin (Figure S6C, S6D; Haverkamp et al., 2005; Wang et al., 2011). This correspondence may provide clues to the spatial patterning of F-RGCs.

Foxp2 RGCs in primate retina

Finally, we asked whether combinatorial expression of Foxp and Brn3 transcription factors marks subsets of RGCs in primates as it does in mice. We first stained sections of adult macaque (*Macaca mulatta*) retina with antibodies to Foxp1, Foxp2, Brn3a, Brn3b, and Brn3c. All five proteins were expressed by subsets of cells located in the ganglion cell layer (Figure 7A, 7B). All of these cells were RGCs as assessed by co-expression of RBPMS and

the glutamate transporter vGlut2, which mark RGCs; none expressed the amacrine cell marker Ap2 (Figure 7A, S7A, and data not shown).

Because the Foxp-RGC subsets were sparse, we used whole mounts of parafoveal retina to assay patterns of co-expression with each other and with Brn3 proteins (Figure 7C and S7B). In macaques, as in mice, we found both $Foxp1^+/Foxp2^+$ and $Foxp1^-/Foxp2^+$ RGC populations. In addition, macaque retina bore $Foxp1^+/Foxp2^-$ RGCs, which we also observed in mice, albeit infrequently. Each of these groups expressed at least one Brn3 factor: all $Foxp1^+$ RGCs (both $Foxp1^+/Foxp2^-$ and $Foxp1^+/Foxp2^+$) were $Brn3b^+$, and all $Foxp1^-/Foxp2^+$ RGCs were both Brn3a and Brn3b-positive. Some, but not all, of the $Foxp2^+$ RGCs (both $Foxp1^-/Foxp2^+$ and $Foxp1^+/Foxp2^+$) were also Brn3c-positive. Together, combinatorial expression of Foxp and Brn3 factors defined 5 sets of RGCs in macaque parafoveal retina (Figure 7D). We provisionally refer to these groups as F1-5. Patterns of Foxp and Brn3 expression in F2 and F3 are identical to those in mouse ON-F-RGCs.

We performed DRP analysis to determine whether any of the Foxp-expressing groups in macaque corresponded to authentic types. As expected, all $Foxp2^+$ RGCs taken together exhibited near-random spacing (Figure 7E), suggesting they include multiple RGC types. However, F3 and F4 exhibited regular mosaic patterns (Figure 7E and S7C). The density of F1 and F5 cells was too low to permit decisive conclusions, and F2 appeared to comprise at least 2 types (data not shown).

Because F-RGCs are distributed anisotropically in mouse retina, we asked if the spatial density of $Foxp2^+$ RGCs also varied within the parafoveal region of macaque retina. The total density of RGCs varied little over the first 4 mm from the fovea, consistent with previous reports (Watanabe and Rodieck, 1989). However, the fraction of all RGCs that were $Foxp2^+$ declined ~3-fold over that distance (Figure 7F, 7G, and S7D). This pattern is similar to that reported for midget RGCs but differs from that of other RGC types studied to date (see Discussion).

Discussion

We have described F-RGCs, a set of four RGC types in mouse that have not, to our knowledge, been defined or characterized in detail previously. Their main features are summarized in Figure S8. At least five properties of these cells are noteworthy: (1) they form ON/OFF symmetrical pairs; (2) they display anisotropies in abundance and size across the receptive field; and two of the types are (3) remarkably abundant, (4) direction-selective, and (5) among the smallest mouse RGCs identified to date. We also show that intersectional patterns of transcription factor expression used to define F-RGC types in mice also mark discrete RGC types in primate retina.

F-RGCs are abundant

Only around half of mouse RGCs have been categorized to date, and we have genetic access to only a fraction of those (Sanes and Masland, 2015). F-RGCs comprise ~25% of all RGCs in central/ventral retina, halving the number of RGCs that remain to be characterized and doubling the number to which we have genetic access.

The abundance of F-mini RGCs is ~4-fold greater than that of the F-midi types, with F-mini[ON] and F-mini[OFF] RGCs each comprising about 8% of all RGCs (16% combined). Thus, they are among the most numerous RGC types in the mouse retina. For comparison, each alpha- and ooDSGC type accounts for 1–2% and 3–4% of total RGCs, respectively (Kay et al., 2011; Sanes and Masland, 2015; Figure 1E). F-mini[ON], F-mini[OFF] and W3B RGCs (Zhang et al., 2012) each reach a similar density of 350 cells/mm^2 in central/ventral retina, together accounting for a third of all RGCs in this region.

Given this prevalence, it is natural to wonder why these cells have apparently escaped detection in a tissue as intensively studied as mouse retina. Several surveys have been published in which large numbers of individual mouse RGCs were labeled in nominally unbiased ways and characterized light microscopically (Badea and Nathans, 2011; Coombs et al., 2007; Kong et al., 2005; Sümbül et al., 2014; Sun et al., 2002; Völgyi et al., 2009), as well as studies focused specifically on DSGCs (Briggman and Euler, 2011; Gauvain and Murphy, 2015; Vlasits et al., 2014). Oddly, none of the types described in these studies show a clear correspondence to any F-RGC types, although "Cluster 4" cells described by Kong et al (2005) and "cell o" described by Badea and Nathan (2011) show some morphological similarity to the F-midi[ON] and F-midi[OFF] cells, respectively. One possibility is that, lacking molecular markers, they were lumped with other types. With respect to the F-mini cells, their small size might have led to their being underrepresented in some surveys. In addition, in one study, the F-mini[OFF] RGCs may have been misidentified as J-RGCs (Farrow et al., 2013), owing to their similar lamination pattern and ventral asymmetry. However, J-RGCs do not express Foxp2 and are clearly a distinct type. Finally, Gauvain and Murphy recently identified a population of SC-projecting ON-DSGCs; these cells have relatively large and radially symmetric dendritic fields, and are thus unlikely to include F-mini[ON] RGCs (Gauvain and Murphy, 2015).

F-mini RGCs are direction-selective

It remains unclear whether direction-selective units in higher image-forming centers, such as superior colliculus, dorsal lateral geniculate nucleus, and visual cortex, inherit their selectivity from direction-selective RGCs in retina or compute it de novo (Cruz-Martín et al., 2014; Inayat et al., 2015; Marshel et al., 2012; Priebe et al., 2006; Rochefort et al., 2011).

Discussions of this issue in mouse have focused on five previously identified direction-selective RGCs that project to image-forming centers: four types of ooDSGCs, which are similar in structure and physiological properties, but differ in preferred directions (ventral, dorsal, nasal and temporal; (Borst and Helmstaedter, 2015; Vaney et al., 2012) and ventrally-preferring J-RGCs, the single population of OFF direction-selective RGCs identified to date (Kim et al., 2008, 2010). Sparse populations of ON direction-selective RGCs have also been identified, but they project to accessory rather than image-forming areas (Dhande et al., 2013; Sanes and Masland, 2015). It remains unclear whether SC-projecting ON-DSGCs described by Gauvain and Murphy also target image-forming regions of the thalamus (Gauvain and Murphy, 2015). In contrast F-mini[ON] DSGCs project to both dLGN and SC, and F-mini[OFF] RGCs are at least twice as numerous as J-RGCs. Moreover, the selectivity with which F-RGCs target the lateral shell of the dLGN marks an intriguing parallel to the recent findings of Cruz-Martin and colleagues, who define this region as the DSGC-recipient

zone, in which di-synaptic circuits link DSGCs directly to visual cortex (Cruz-Martín et al., 2014). Finally, the abundance of the F-mini RGCs nearly doubles the fraction of DS cells among all RGCs, and may account for the bias for vertical motion selectivity observed within the superior colliculus in some studies (Dräger and Hubel, 1975; Inayat et al., 2015).

Previously studied direction-selective RGCs compute direction in different ways. Dendritic asymmetry and the asymmetry of surround inhibition are critical for J-RGCs, whereas direction-selective input from starburst amacrine cells plays a predominant role in ooDSGCs and ON-DSGCs (Vaney et al., 2012). Trenholm and colleagues recently reported an intrinsic mechanism for direction-selectivity of ventral-preferring ooDSGCs based predominately on dendritic asymmetry, independent of their input from starburst amacrine cells (Trenholm et al., 2011). F-mini-RGCs have markedly asymmetric dendritic arbors and do not co-stratify significantly with starbursts, suggesting greater parallels with J-RGC and ventral-preferring ooDSGCs than with other DSGC types. Nonetheless, the mechanism by which F-mini-RGCs compute direction remains to be determined.

F-RGCs comprise paramorphic pairs

The F-RGC types can be viewed as forming pairs in either of two senses: both ON and OFF groups comprise mini-midi pairs, and both mini and midi groups comprise ON-OFF pairs. Of these we view the ON-OFF pairing as more compelling because it corresponds to an important organizational principle in retinas of higher mammals: that many individual channels are duplicated to generate ON and OFF representations of each feature detector. This phenomenon, termed paramorphism, is prominent in the primate, rabbit, and cat retina (Berson, 2008; Famiglietti, 2004, 2005; Famiglietti and Kolb, 1976; Wässle et al., 1981, 1983). Paramorphism has not, however, been previously documented for mouse RGCs, which limits the range of methods available for studying its developmental origin. The two F-mini types are similar to each other in many respects including size, dendritic asymmetry, abundance and physiological properties. Thus, they qualify as paramorphic pairs. The same is true for the two F-midi types, although they differed in their light responses (transient vs. sustained). Such physiological divergence may reflect subtle circuit asymmetries, which have been observed among otherwise parallel channels in other species, as well as in mouse (Murphy and Rieke, 2006; Zaghloul et al., 2003).

Finally, the phenomenon of paramorphism leads to the idea that a small alteration in developmental program could lead to duplication and diversification of types. In this regard it is intriguing that Foxp1 is expressed by the OFF but not the ON member of each pair of F-RGCs. Foxp1 plays roles in diversification of neuronal subsets in other systems. In spinal cord, for example, Foxp1 is expressed selectively by limb-innervating motor neurons, and plays a key role in their differentiation from Foxp1-negative hypaxial motor neurons during development (Dasen et al., 2008; Rousso et al., 2008). We speculate that in mouse retina, Foxp1 could serve as part of a related program of RGC diversification. Genetic reagents are available to test this idea.

F-RGCs are anisotropic in size and distribution

In many vertebrates, visual information is sampled non-uniformly across the visual field, with RGC densities increasing within anatomically distinct regions, such as the area centralis in cats or the fovea in primates. Until recently, the distribution of RGCs in mice was thought to be nearly invariant across the retina, suggesting uniform spatial sampling (Huberman and Niell, 2011; Jeon et al., 1998). However recent studies have challenged this idea (Bleckert et al., 2014; Hughes et al., 2013; Zhang et al., 2012). We show that all F-RGCs exhibit non-uniform spatial topographies. Interestingly, however, their anisotropy is itself non-uniform: F-mini RGCs are arranged in a shallow ventral to dorsal gradient (ventral high), F-midi[OFF] RGCs form a steeper gradient in the same direction, and F-midi[ON] RGCs form a dorsal to ventral gradient. Combined with previously reported anisotropies (temporal-high for alpha RGCs, central/ventral high for W3B-RGCs, dorsal high for ip-RGCs; Bleckert et al., 2014; Hughes et al., 2013; Zhang et al., 2012) our results demonstrate a bewildering set of specializations in mouse retina.

F-RGCs of mice and monkeys

A challenge for visual neuroscience –indeed, neuroscience generally– is to extend the cell type classification enterprise from model organisms such as mice to primates. We asked whether the patterns of Foxp and Brn3 isoform expression that defined F-RGCs in mice also labeled discrete subsets of cells in macaque retina. Indeed, we identified five groups of RGCs that each express at least one Foxp and at least one Brn3 protein. Although these groups remain to be characterized, their existence encourages the view that classification schemes derived from and validated in mice will be useful for understanding primate retina.

Importantly, of all 32 (2^5) possible combination of Foxp and Brn3 factors, we observed only four in mice and five in macaque. Moreover, the combinations observed in mouse F-mini[ON] and F-mini[OFF] RGCs are identical to those observed in macaque F2 and F3 RGCs, respectively. These patterns support the ideas that Foxp and Brn3 factors play developmental roles in specification of these cells, and that there is an evolutionary relationship between Foxp-expressing macaque and mouse RGCs. These roles and relationships remain to be investigated, but a particularly intriguing parallel is that between mouse F-RGCs and arguably the best studied RGC group in primates, midget RGCs (Berson, 2008; Silveira et al., 2004). F-mini-RGCs in mice and midget RGCs in primates are the smallest and most abundant types in their respective species, both have highly-branched and tufted dendrites, both are asymmetric, and both form "paramorphic" ON-OFF pairs.

Could primate Foxp2^{+} RGCs be midgets? A precise correspondence is unlikely for at least two reasons. First, primate midget RGCs have so far not been reported to be direction-selective, although we are unaware of critical tests of this possibility in peripheral retina, where their receptive fields are sufficiently large to support such a computation (Crook et al., 2011; Silveira et al., 2004). Second, Foxp2^{+} RGCs comprise only ~2% of RGCs in primate parafoveal retina, whereas midget RGCs comprise ~90% of RGCs in this region. On the other hand, the distribution of Foxp2^{+} RGCs is remarkably similar to that of midget RGCs: highest near the fovea and declining in proportion with distance. Another abundant class, parasol RGCs, as well as rare classes of which we are aware, increase in fractional

representation with distance from the fovea ([Watanabe and Rodieck, 1989]). In addition, the anisotropy and asymmetry of midgets (fovea-oriented) is strikingly similar to that of F-mini[ON] RGCs, which are oriented dorsally in ventral retina and ventrally in dorsal retina. Thus, an intriguing hypothesis is that midget RGCs are heterogeneous and that macaque Foxp-positive RGCs comprise a few of multiple midget subtypes.

Experimental Procedures

Animals

Cdh4[CreER] and *Cdh13[CreER]* mice were generated by targeted insertion of a frt-neo-frt cassette, a 6xmyc-tagged CreER-T2, and poly-adenylation signal at the translational start site of the *Cdh4* and *13* coding sequences, respectively, as described previously for *Cdh6[CreER]* mice ([Kay et al., 2011]). This removed the N-terminal 19 amino acids (MTTGSVLPLLLLGLSGALR) of *Cadherin 4* protein, and the N-terminal 15 amino acids (MQPRTPLTLCVLLSQ) of *Cadherin 13*. Chimeras were produced by the Harvard University Genome Modification Facility. *Foxp2[Cre]* mice were generated by targeted insertion of a frt-neo-frt cassette, internal ribosomal entry sequence, and Cre:GFP fusion sequence at a site just downstream of the endogenous translational stop codon in exon 19 of the *Foxp2* gene. To excise the frt-neo-frt cassette, mice were crossed with mice expressing flp recombinase ubiquitously ([Farley et al., 2000; Rodríguez et al., 2000]). *JAMB[CreER]*, *Cdh6[CreER]*, *TYWY3*, *TYWY7*, and *Thy1-stop-YFP* lines were generated in our laboratory and have been described previously ([Buffelli et al., 2003; Kim et al., 2008; Kim et al., 2010; Kay et al., 2011; Krishnaswamy et al., 2015]). *Cdh3-GFP* BAC transgenic mice ([Osterhout et al., 2011]) were generated in the Gensat project and obtained from the Mutant Mouse Resource and Research Center (https://www.mmrrc.org/). *PV[Cre]* and HB9-GFP mice ([Trenholm et al., 2011]) were obtained from Jackson Labs. *PV[Cre]*, *Cdh4[CreER]* and *Cdh13[CreER]* mice were crossed with reporter mice containing a *lox-stop-lox-YFP* cassette ([Buffelli et al., 2003]). Tamoxifen (2 mg to 8 mg, Sigma) was injected intraperitoneally into double transgenic mice, either neonatally or in adults, to label cells. AAV-delivery of a flex-GFP cassette was used to label cells in *Foxp2[Cre]* mice. All mice were maintained on a C57BL6 background. All procedures were performed in accordance with Harvard IACUC protocols.

Histology

Retinas were prepared for whole mount or cryosection analysis as described previously ([Kim et al., 2010]). Thick brain sections were stained and optically cleared using CUBIC reagent #1 ([Susaki et al., 2014]). To label F-RGCs and their projections, AAV containing a flex-GFP cassette (University of Pennsylvania) was injected intravitreally into *Foxp2[Cre]* mice. See Supplemental Experimental Procedures for detailed histological procedures, antibody information, and protocols for image analysis.

Electrophysiology

Electrophysiological analysis was performed as described previously ([Kostadinov and Sanes, 2015]), with minor modifications described in Supplemental Experimental Procedures.

Statistical Analysis

Unless otherwise stated, all data are presented as mean ± SE. Spatial statistics were computed using WinDRP software, which performs DRP and nearest-neighbor calculations on cells within and between populations (Euler, 2003; Kay et al., 2012; Rockhill et al., 2000). For morphological and physiological comparisons, a two-tailed t-test was used to assess statistical significance (p>0.05) between experimental groups. Further details on spatial and morphological statistics are included in Supplemental Experimental Procedures.

Supplementary Material

Refer to Web version on PubMed Central for supplementary material.

Acknowledgments

References

Badea TC, Nathans J. Quantitative analysis of neuronal morphologies in the mouse retina visualized by using a genetically directed reporter. J Comp Neurol. 2004; 480:331–351. [PubMed: 15558785]

Badea TC, Nathans J. Morphologies of mouse retinal ganglion cells expressing transcription factors Brn3a, Brn3b, and Brn3c: analysis of wild type and mutant cells using genetically-directed sparse labeling. Vision Res. 2011; 51:269–279. [PubMed: 20826176]

Baden T, Berens P, Franke K, Román Rosón M, Bethge M, Euler T. The functional diversity of retinal ganglion cells in the mouse. Nature. 2016; 529:345–350. [PubMed: 26735013]

Benito-Gonzalez A, Alvarez FJ. Renshaw cells and Ia inhibitory interneurons are generated at different times from p1 progenitors and differentiate shortly after exiting the cell cycle. J Neurosci. 2012; 32:1156–1170. [PubMed: 22279202]

Berson, DM. In The Senses: A Comprehensive Reference. Elsevier; 2008. Retinal Ganglion Cell Types and Their Central Projections; p. 491-519.

Bisgrove DA, Godbout R. Differential expression of AP-2alpha and AP-2beta in the developing chick retina: repression of R-FABP promoter activity by AP-2. Dev Dyn. 1999; 214:195–206. [PubMed: 10090146]

Bleckert A, Schwartz GW, Turner MH, Rieke F, Wong ROL. Visual space is represented by nonmatching topographies of distinct mouse retinal ganglion cell types. Curr Biol. 2014; 24:310–315. [PubMed: 24440397]

Borst A, Helmstaedter M. Common circuit design in fly and mammalian motion vision. Nat Neurosci. 2015; 18:1067–1076. [PubMed: 26120965]

Briggman KL, Euler T. Bulk electroporation and population calcium imaging in the adult mammalian retina. J Neurophysiol. 2011; 105:2601–2609. [PubMed: 21346205]

Buffelli M, Burgess RW, Feng G, Lobe CG, Lichtman JW, Sanes JR. Genetic evidence that relative synaptic efficacy biases the outcome of synaptic competition. Nature. 2003; 424:430–434. [PubMed: 12879071]

Carcieri SM, Jacobs AL, Nirenberg S. Classification of retinal ganglion cells: a statistical approach. J Neurophysiol. 2003; 90:1704–1713. [PubMed: 12966177]

Catela C, Shin MM, Dasen JS. Assembly and Function of Spinal Circuits for Motor Control. Annu Rev Cell Dev Biol. 2015

Coombs JL, Van Der List D, Chalupa LM. Morphological properties of mouse retinal ganglion cells during postnatal development. J Comp Neurol. 2007; 503:803–814. [PubMed: 17570502]

Crook JD, Manookin MB, Packer OS, Dacey DM. Horizontal cell feedback without cone type-selective inhibition mediates "red-green" color opponency in midget ganglion cells of the primate retina. J Neurosci. 2011; 31:1762–1772. [PubMed: 21289186]

Cruz-Martín A, El-Danaf RN, Osakada F, Sriram B, Dhande OS, Nguyen PL, Callaway EM, Ghosh A, Huberman AD. A dedicated circuit links direction-selective retinal ganglion cells to the primary visual cortex. Nature. 2014; 507:358–361. [PubMed: 24572358]

Dacey DM, Packer OS. Colour coding in the primate retina: diverse cell types and cone-specific circuitry. Curr Opin Neurobiol. 2003; 13:421–427. [PubMed: 12965288]

Dasen JS, De Camilli A, Wang B, Tucker PW, Jessell TM. Hox repertoires for motor neuron diversity and connectivity gated by a single accessory factor, FoxP1. Cell. 2008; 134:304–316. [PubMed: 18662545]

Dhande OS, Huberman AD. Retinal ganglion cell maps in the brain: implications for visual processing. Curr Opin Neurobiol. 2014; 24:133–142. [PubMed: 24492089]

Dhande OS, Estevez ME, Quattrochi LE, El-Danaf RN, Nguyen PL, Berson DM, Huberman AD. Genetic dissection of retinal inputs to brainstem nuclei controlling image stabilization. J Neurosci. 2013; 33:17797–17813. [PubMed: 24198370]

Dräger UC, Hubel DH. Responses to visual stimulation and relationship between visual, auditory, and somatosensory inputs in mouse superior colliculus. J Neurophysiol. 1975; 38:690–713. [PubMed: 1127462]

Duan X, Qiao M, Bei F, Kim IJ, He Z, Sanes JR. Subtype-specific regeneration of retinal ganglion cells following axotomy: effects of osteopontin and mTOR signaling. Neuron. 2015; 85:1244–1256. [PubMed: 25754821]

Euler, T. WinDRP website. 2003. http://wvad.mpimf-heidelberg.mpg.de/abteilungen/biomedizinischeOptik/software/WinDRP/index.html

Famiglietti EV. Class I and class II ganglion cells of rabbit retina: a structural basis for X and Y (brisk) cells. J Comp Neurol. 2004; 478:323–346. [PubMed: 15384072]

Famiglietti EV. "Small-tufted" ganglion cells and two visual systems for the detection of object motion in rabbit retina. Vis Neurosci. 2005; 22:509–534. [PubMed: 16212708]

Famiglietti EV, Kolb H. Structural basis for ON-and OFF-center responses in retinal ganglion cells. Science. 1976; 194:193–195. [PubMed: 959847]

Farley FW, Soriano P, Steffen LS, Dymecki SM. Widespread recombinase expression using FLPeR (flipper) mice. Genesis. 2000; 28:106–110. [PubMed: 11105051]

Farrow K, Teixeira M, Szikra T, Viney TJ, Balint K, Yonehara K, Roska B. Ambient illumination toggles a neuronal circuit switch in the retina and visual perception at cone threshold. Neuron. 2013; 78:325–338. [PubMed: 23541902]

Gauvain G, Murphy GJ. Projection-specific characteristics of retinal input to the brain. J Neurosci. 2015; 35:6575–6583. [PubMed: 25904807]

Hattar S, Liao HW, Takao M, Berson DM, Yau KW. Melanopsin-containing retinal ganglion cells: architecture, projections, and intrinsic photosensitivity. Science. 2002; 295:1065–1070. [PubMed: 11834834]

Haverkamp S, Wässle H, Duebel J, Kuner T, Augustine GJ, Feng G, Euler T. The primordial, blue-cone color system of the mouse retina. J Neurosci. 2005; 25:5438–5445. [PubMed: 15930394]

Hisaoka T, Nakamura Y, Senba E, Morikawa Y. The forkhead transcription factors, Foxp1 and Foxp2, identify different subpopulations of projection neurons in the mouse cerebral cortex. Neuroscience. 2010; 166:551–563. [PubMed: 20040367]

Huberman AD, Niell CM. What can mice tell us about how vision works? Trends Neurosci. 2011; 34:464–473. [PubMed: 21840069]

Huberman AD, Manu M, Koch SM, Susman MW, Lutz AB, Ullian EM, Baccus SA, Barres BA. Architecture and activity-mediated refinement of axonal projections from a mosaic of genetically identified retinal ganglion cells. Neuron. 2008; 59:425–438. [PubMed: 18701068]

Huberman AD, Wei W, Elstrott J, Stafford BK, Feller MB, Barres BA. Genetic identification of an On-Off direction-selective retinal ganglion cell subtype reveals a layer-specific subcortical map of posterior motion. Neuron. 2009; 62:327–334. [PubMed: 19447089]

Hughes S, Watson TS, Foster RG, Peirson SN, Hankins MW. Nonuniform distribution and spectral tuning of photosensitive retinal ganglion cells of the mouse retina. Curr Biol. 2013; 23:1696–1701. [PubMed: 23954426]

Inayat S, Barchini J, Chen H, Feng L, Liu X, Cang J. Neurons in the most superficial lamina of the mouse superior colliculus are highly selective for stimulus direction. J Neurosci. 2015; 35:7992–8003. [PubMed: 25995482]

Isayama T, O'Brien BJ, Ugalde I, Muller JF, Frenz A, Aurora V, Tsiaras W, Berson DM. Morphology of retinal ganglion cells in the ferret (Mustela putorius furo). J Comp Neurol. 2009; 517:459–480. [PubMed: 19790267]

Jeon CJ, Strettoi E, Masland RH. The major cell populations of the mouse retina. J Neurosci. 1998; 18:8936–8946. [PubMed: 9786999]

Kay JN, De la Huerta I, Kim I-J, Zhang Y, Yamagata M, Chu MW, Meister M, Sanes JR. Retinal ganglion cells with distinct directional preferences differ in molecular identity, structure, and central projections. J Neurosci. 2011; 31:7753–7762. [PubMed: 21613488]

Kay JN, Chu MW, Sanes JR. MEGF10 and MEGF11 mediate homotypic interactions required for mosaic spacing of retinal neurons. Nature. 2012; 483:465–469. [PubMed: 22407321]

Kim IJ, Zhang Y, Yamagata M, Meister M, Sanes JR. Molecular identification of a retinal cell type that responds to upward motion. Nature. 2008; 452:478–482. [PubMed: 18368118]

Kim I-J, Zhang Y, Meister M, Sanes JR. Laminar restriction of retinal ganglion cell dendrites and axons: subtype-specific developmental patterns revealed with transgenic markers. J Neurosci. 2010; 30:1452–1462. [PubMed: 20107072]

Kong J-H, Fish DR, Rockhill RL, Masland RH. Diversity of ganglion cells in the mouse retina: unsupervised morphological classification and its limits. J Comp Neurol. 2005; 489:293–310. [PubMed: 16025455]

Kostadinov D, Sanes JR. Protocadherin-dependent dendritic self-avoidance regulates neural connectivity and circuit function. Elife. 2015; 4

Krishnaswamy A, Yamagata M, Duan X, Hong YK, Sanes JR. Sidekick 2 directs formation of a retinal circuit that detects differential motion. Nature. 2015; 524:466–470. [PubMed: 26287463]

Lodato S, Arlotta P. Generating Neuronal Diversity in the Mammalian Cerebral Cortex. Annu Rev Cell Dev Biol. 2015

Marshel JH, Kaye AP, Nauhaus I, Callaway EM. Anterior-posterior direction opponency in the superficial mouse lateral geniculate nucleus. Neuron. 2012; 76:713–720. [PubMed: 23177957]

Masland RH. The neuronal organization of the retina. Neuron. 2012; 76:266–280. [PubMed: 23083731]

de Melo J, Qiu X, Du G, Cristante L, Eisenstat DD. Dlx1, Dlx2, Pax6, Brn3b, and Chx10 homeobox gene expression defines the retinal ganglion and inner nuclear layers of the developing and adult mouse retina. J Comp Neurol. 2003; 461:187–204. [PubMed: 12724837]

Morin LP, Studholme KM. Retinofugal projections in the mouse. J Comp Neurol. 2014; 522:3733–3753. [PubMed: 24889098]

Murphy GJ, Rieke F. Network variability limits stimulus-evoked spike timing precision in retinal ganglion cells. Neuron. 2006; 52:511–524. [PubMed: 17088216]

Osterhout JA, Josten N, Yamada J, Pan F, Wu S, Nguyen PL, Panagiotakos G, Inoue YU, Egusa SF, Volgyi B, et al. Cadherin-6 mediates axon-target matching in a non-image-forming visual circuit. Neuron. 2011; 71:632–639. [PubMed: 21867880]

Priebe NJ, Lisberger SG, Movshon JA. Tuning for spatiotemporal frequency and speed in directionally selective neurons of macaque striate cortex. J Neurosci. 2006; 26:2941–2950. [PubMed: 16540571]

Reese BE. Retinal Mosaics: Pattern Formation Driven by Local Interactions between Homotypic Neighbors. Frontiers in Neural Circuits. 2012; 6

Rochefort NL, Narushima M, Grienberger C, Marandi N, Hill DN, Konnerth A. Development of direction selectivity in mouse cortical neurons. Neuron. 2011; 71:425–432. [PubMed: 21835340]

Rockhill RL, Euler T, Masland RH. Spatial order within but not between types of retinal neurons. Proc Natl Acad Sci USA. 2000; 97:2303–2307. [PubMed: 10688875]

Rodieck RW. The density recovery profile: a method for the analysis of points in the plane applicable to retinal studies. Vis Neurosci. 1991; 6:95–111. [PubMed: 2049333]

Rodriguez AR, de Sevilla Müller LP, Brecha NC. The RNA binding protein RBPMS is a selective marker of ganglion cells in the mammalian retina. J Comp Neurol. 2014; 522:1411–1443. [PubMed: 24318667]

Rodríguez CI, Buchholz F, Galloway J, Sequerra R, Kasper J, Ayala R, Stewart AF, Dymecki SM. High-efficiency deleter mice show that FLPe is an alternative to Cre-loxP. Nat Genet. 2000; 25:139–140. [PubMed: 10835623]

Rousso DL, Gaber ZB, Wellik D, Morrisey EE, Novitch BG. Coordinated actions of the forkhead protein Foxp1 and Hox proteins in the columnar organization of spinal motor neurons. Neuron. 2008; 59:226–240. [PubMed: 18667151]

Rousso DL, Pearson CA, Gaber ZB, Miquelajauregui A, Li S, Portera-Cailliau C, Morrisey EE, Novitch BG. Foxp-mediated suppression of N-cadherin regulates neuroepithelial character and progenitor maintenance in the CNS. Neuron. 2012; 74:314–330. [PubMed: 22542185]

Sanes JR, Masland RH. The types of retinal ganglion cells: current status and implications for neuronal classification. Annu Rev Neurosci. 2015; 38:221–246. [PubMed: 25897874]

Sanes JR, Zipursky SL. Design Principles of Insect and Vertebrate Visual Systems. Neuron. 2010; 66:15–36. [PubMed: 20399726]

Silveira LC, Saito CA, Lee BB, Kremers J, da Silva Filho M, Kilavik BE, Yamada ES, Perry VH. Morphology and physiology of primate M- and P-cells. Prog Brain Res. 2004; 144:21–46. [PubMed: 14650838]

Sümbül U, Song S, McCulloch K, Becker M, Lin B, Sanes JR, Masland RH, Seung HS. A genetic and computational approach to structurally classify neuronal types. Nat Commun. 2014; 5:3512. [PubMed: 24662602]

Sun W, Li N, He S. Large-scale morphological survey of mouse retinal ganglion cells. J Comp Neurol. 2002; 451:115–126. [PubMed: 12209831]

Susaki EA, Tainaka K, Perrin D, Kishino F, Tawara T, Watanabe TM, Yokoyama C, Onoe H, Eguchi M, Yamaguchi S, et al. Whole-brain imaging with single-cell resolution using chemical cocktails and computational analysis. Cell. 2014; 157:726–739. [PubMed: 24746791]

Szmajda BA, Grünert U, Martin PR. Mosaic properties of midget and parasol ganglion cells in the marmoset retina. Vis Neurosci. 2005; 22:395–404. [PubMed: 16212698]

Tien N-W, Pearson JT, Heller CR, Demas J, Kerschensteiner D. Genetically Identified Suppressed-by-Contrast Retinal Ganglion Cells Reliably Signal Self-Generated Visual Stimuli. J Neurosci. 2015; 35:10815–10820. [PubMed: 26224863]

Trenholm S, Johnson K, Li X, Smith RG, Awatramani GB. Parallel mechanisms encode direction in the retina. Neuron. 2011; 71:683–694. [PubMed: 21867884]

Vaney DI, Sivyer B, Taylor WR. Direction selectivity in the retina: symmetry and asymmetry in structure and function. Nat Rev Neurosci. 2012; 13:194–208. [PubMed: 22314444]

Vlasits AL, Bos R, Morrie RD, Fortuny C, Flannery JG, Feller MB, Rivlin-Etzion M. Visual stimulation switches the polarity of excitatory input to starburst amacrine cells. Neuron. 2014; 83:1172–1184. [PubMed: 25155960]

Voinescu PE, Kay JN, Sanes JR. Birthdays of retinal amacrine cell subtypes are systematically related to their molecular identity and soma position. J Comp Neurol. 2009; 517:737–750. [PubMed: 19827163]

Völgyi B, Chheda S, Bloomfield SA. Tracer coupling patterns of the ganglion cell subtypes in the mouse retina. J Comp Neurol. 2009; 512:664–687. [PubMed: 19051243]

Wang YV, Weick M, Demb JB. Spectral and temporal sensitivity of cone-mediated responses in mouse retinal ganglion cells. J Neurosci. 2011; 31:7670–7681. [PubMed: 21613480]

Wässle H, Boycott BB, Illing RB. Morphology and mosaic of on- and off-beta cells in the cat retina and some functional considerations. Proc R Soc Lond, B, Biol Sci. 1981; 212:177–195. [PubMed: 6166013]

Wässle H, Peichl L, Boycott BB. A spatial analysis of on- and off-ganglion cells in the cat retina. Vision Res. 1983; 23:1151–1160. [PubMed: 6649435]

Watanabe M, Rodieck RW. Parasol and midget ganglion cells of the primate retina. J Comp Neurol. 1989; 289:434–454. [PubMed: 2808778]

Yonehara K, Ishikane H, Sakuta H, Shintani T, Nakamura-Yonehara K, Kamiji NL, Usui S, Noda M. Identification of retinal ganglion cells and their projections involved in central transmission of information about upward and downward image motion. PLoS ONE. 2009; 4:e4320. [PubMed: 19177171]

Zaghloul KA, Boahen K, Demb JB. Different circuits for ON and OFF retinal ganglion cells cause different contrast sensitivities. J Neurosci. 2003; 23:2645–2654. [PubMed: 12684450]

Zeck GM, Masland RH. Spike train signatures of retinal ganglion cell types. Eur J Neurosci. 2007; 26:367–380. [PubMed: 17650112]

Zhang Y, Kim I-J, Sanes JR, Meister M. The most numerous ganglion cell type of the mouse retina is a selective feature detector. Proc Natl Acad Sci USA. 2012; 109:E2391–2398. [PubMed: 22891316]

Highlights

- Foxp2 expression marks F-RGCs, 2 mini and 2 midi types comprising 2 pairs

- Intersectional expression of Foxp and Brn3 genes uniquely identifies each F-RGC type

- The two F-mini RGC types are unusually small, abundant and direction-selective

- Combinatorial expression of Foxp and Brn3 genes also marks RGC types in macaque retina
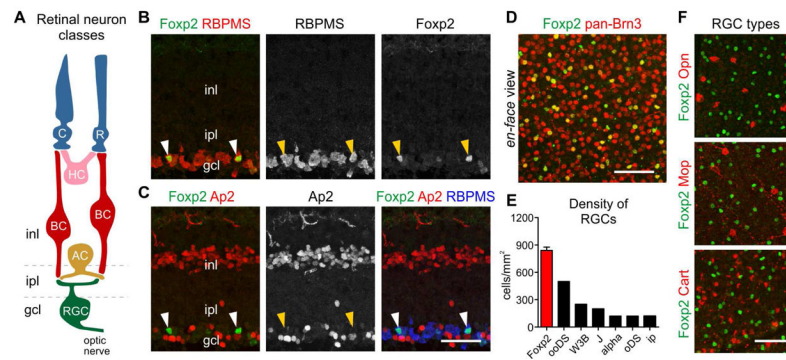
Figure 1. Foxp2 expression distinguishes F-RGCs from currently known types

(A) Model showing the major neuronal classes in the retina. R, rods; C, cones; HC, horizontal cells; BC, bipolar cells; AC, amacrine cells; RGC, retinal ganglion cells; inl, inner nuclear layer; ipl, inner plexiform layer; gcl, ganglion cell layer.

(B, C) Antibody staining analysis for Foxp2 plus molecular markers for RGCs, RBPMS (B), and amacrine cells, Ap2 (C), in the adult mouse retina. Arrows point to the same cells in each panel.

(D) Immunostaining for Foxp2 combined with antibodies to all three Brn3-transcription factors (a, b, c; "pan-Brn3").

(E) Density of Foxp2 RGCs as a group compared to that of molecularly defined RGC types (from Sanes and Masland, 2015).

(F) Analysis of Foxp2 RGCs combined with markers for the following RGC types: Osteopontin, alpha-RGCs (top); Melanopsin, ip-RGCs (middle); and Cart, ooDSGCs (bottom).

All images are taken from the central/ventral region of the retina. Scale bars in (B, C) = 50 μm; (D, F) = 100 μm. See also Figure S1.
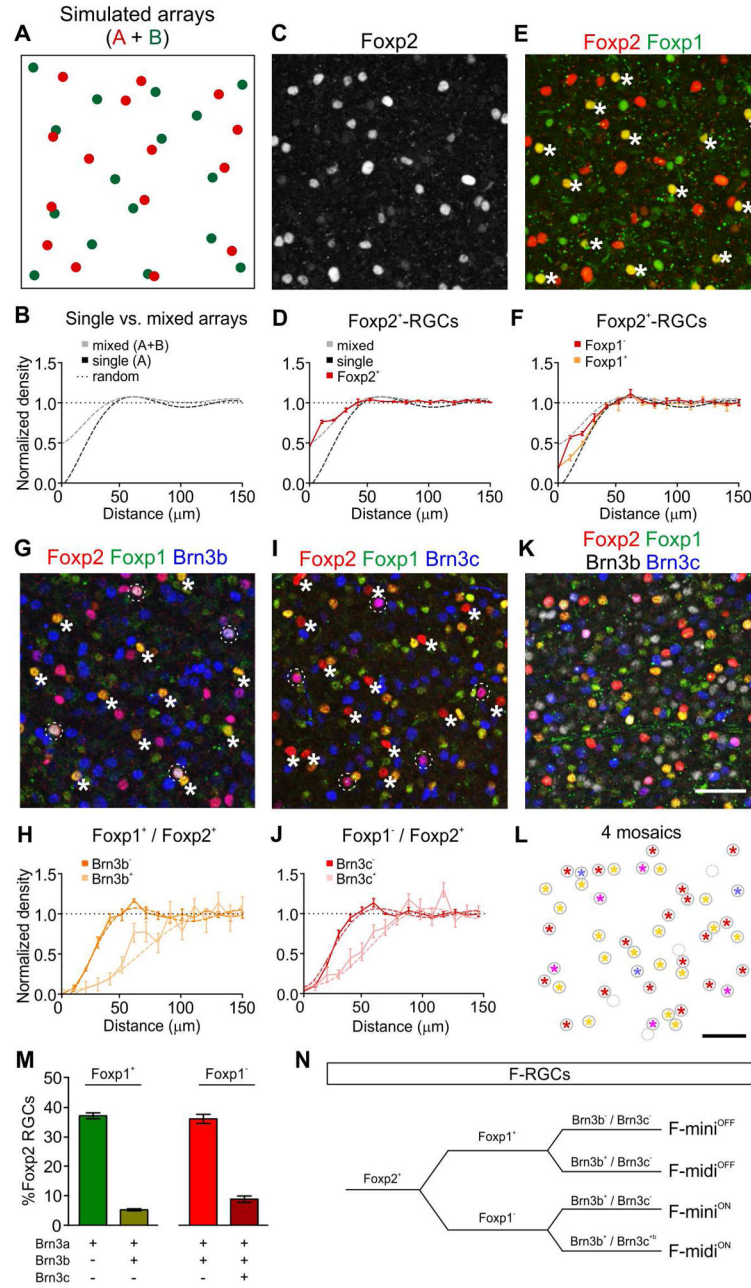
Figure 2. Combinatorial expression of transcription factors divide F-RGCs into 4 types
(A) Retinal mosaics modeled as close-packed hexagonal arrays with positional jitter. Dots represent single arrays (red or green) of the same side-length as defined by Zhang et al. (2012).

(B) DRP on a single array (A → A; black dashed line) produces a slope that scales with side-length. DRP on a mixture of 2 arrays (A+B → A+B; grey dashed line) of the same side-length produces a slope mid-way between a random distribution and a single array, allowing for calculation of the fraction f of an array labeled (f < 1, partial array; f > 1, mixture of arrays). Random distribution is represented by the dotted line.

(C, D) Immunolabeling of Foxp2 in adult mouse retina (C). DRP of total Foxp2 RGCs is that of a mixed array with f = 2.2 (D).

(E, F) Foxp1 divides Foxp2 RGCs into 2 groups (E). DRP on Foxp1$^+$ F-RGCs (orange line) and Foxp1$^-$ F-RGCs (red line) are compared to that of a mixture of 2 arrays (gray dashed line) and a single array of the same side length (black dashed line) (F).

(G, H) Brn3b divides Foxp1$^+$ F-RGCs into 2 types, one abundant (Foxp1$^+$/Foxp2$^+$/Brn3b$^-$; asterisks), and one sparse (Foxp1$^+$/Foxp2$^+$/Brn3b$^+$; dashed circles) (G). DRP of abundant (orange line) and sparse (peach line) Foxp1$^+$ F-RGCs resemble matched single arrays of similar side-lengths (dashed lines), indicating they each form a single array, with f ≈ 1 (H).

(I, J) Brn3c divides Foxp1$^-$ F-RGCs into two types, one abundant (Foxp1$^-$/Foxp2$^+$/Brn3c$^-$; asterisks) and one sparse (Foxp1$^-$/Foxp2$^+$/Brn3c$^+$; dashed circles) (I). DRP of abundant (red line) and sparse (pink line) Foxp1$^-$ F-RGCs resemble matched single arrays of similar side-lengths (dashed lines), indicating they each form a single array, with f ≈ 1 (J).

(K, L) Quadruple immunolabeling with Foxp1, Foxp2, Brn3b, and Brn3c marks the four F-RGC types simultaneously (K). Colored asterisks represent the relative position and identity of molecularly defined F-RGC types (L). Red, F-mini^{ON}; yellow, F-mini^{OFF}; purple, F-midi^{ON}; cyan, F-midi^{OFF}. Empty dotted circles indicate dim cells which were not categorized.

(M) Contribution of each F-RGC type to the total Foxp2$^+$ RGC population. n = 4 retinas from 4 animals per type. Scale bar = 50 μm.

(N) Dendogram showing the four molecularly defined F-RGC types and their combinatorial TFs. See also Figure S2.
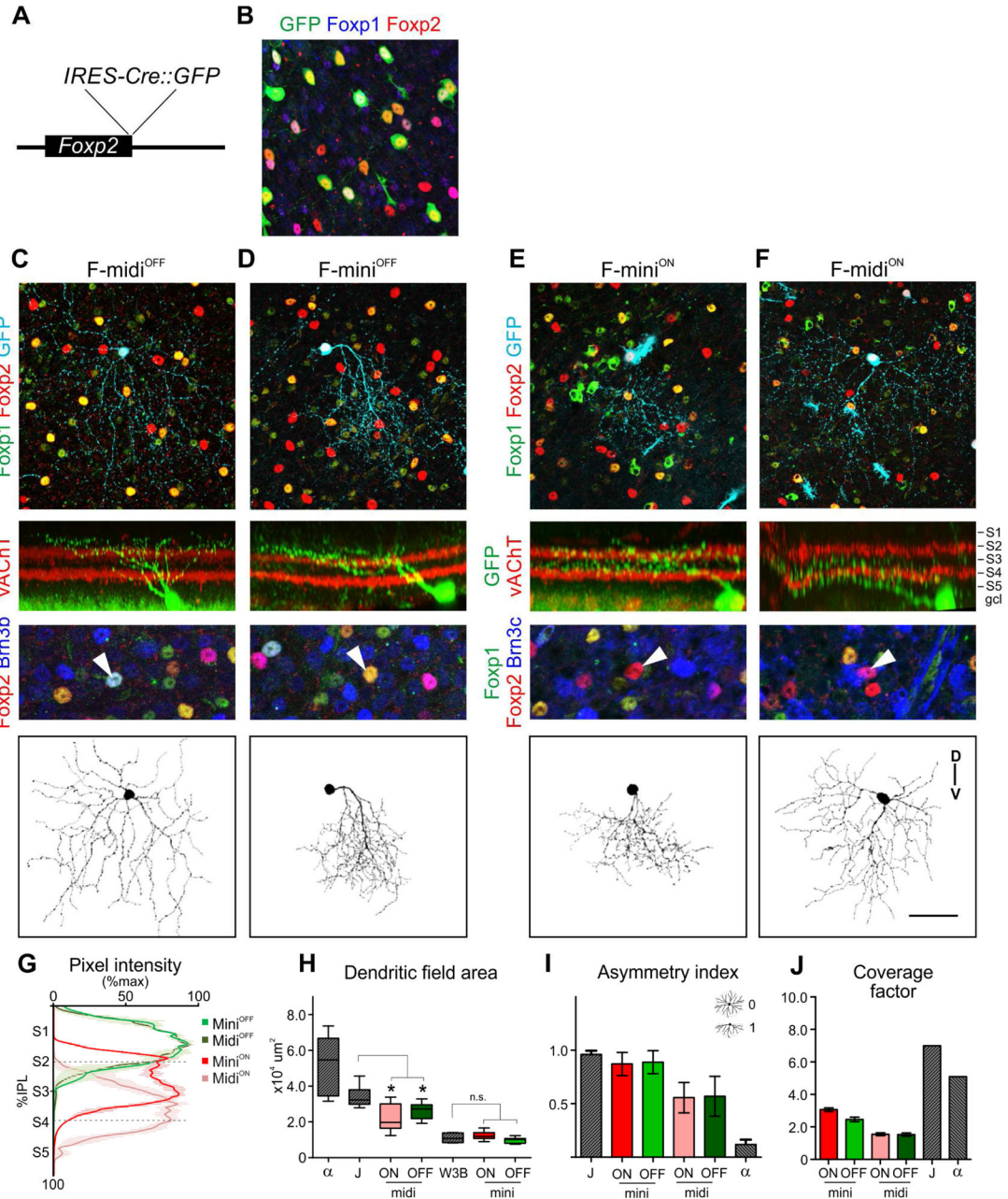
Figure 3. Morphological characterization of F-RGCs

(A) Schematic of the *Foxp2-ires-Cre:GFP (Foxp2^Cre)* allele.

(B) Immunostaining for Foxp2, Foxp1, and GFP in adult *Foxp2^Cre* retinas following intravitreal injection of high-titer *AAV2/9^flexGFP*. Only infected Foxp2+ RGCs are labeled.

(C–F) Injection of low-titer *AAV2/9^flexGFP* into *Foxp2-Cre* mice reveals 4 morphologically distinct types that correspond to discrete molecular identities: F-midi^OFF, Foxp2+/Foxp1+/Brnb+ (C) F-mini^OFF, Foxp2+/Foxp1+/Brnb− (D) F-mini^ON, Foxp2+/Foxp1−/Brn3c− (E) F-midi^ON, Foxp2+/Foxp1−/Brn3c+ (F).

(G) Dendritic stratification depth of individually segmented F-RGC types. n = 5–7 cells per type.

(H) Box plot of dendritic field areas for indicated RGC types. W3B and F-mini^{ON} RGCs are similar in size whereas F-mini^{OFF} RGCs tended to be smaller with a trend toward significance (p = 0.07).

(I) Analysis of dendritic asymmetry calculated for indicated RGC types (0 = perfect symmetry; 1 = perfect asymmetry.

(J) Dendritic coverage factor (CF) for F-RGCs.

Data for J-, W3B, and alpha- RGC types from Kim et al., 2008, 2010. n = 7–15 cells per type. *, p<0.05, two-tailed t-test. Scale bar in (C–F, bottom row) = 50 μm. See also Figure S3.
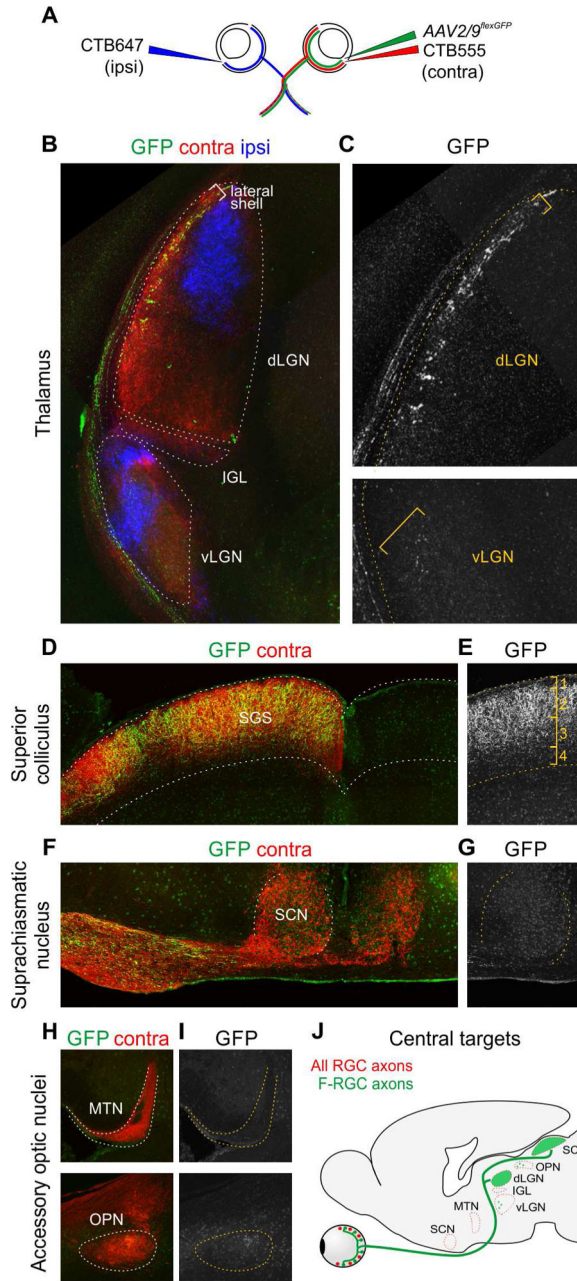
Figure 4. F-RGC axons selectively innervate image-forming visual targets in the brain
(A–I) F-RGC central projections revealed by intravitreal injection of *AAV2/9flexGFP* and fluorophore-conjugated cholera toxin b (CTB) in adult *Foxp2Cre* mice (A). Sections are from dorsal and ventral lateral geniculate nuclei and intergeniculate leaflet of the thalamus (dLGN, vLGN, IGL; B,C); stratum griseum superficiale of the superior colliculus (SGS; D, E); suprachiasmatic nucleus (SCN; F,G); medial terminal nucleus (MTN, top) and olivary pretectal nucleus (OPN, bottom) (H, I). Images are representative from n = 4 animals. (J) Schematic of F-RGC central projections.
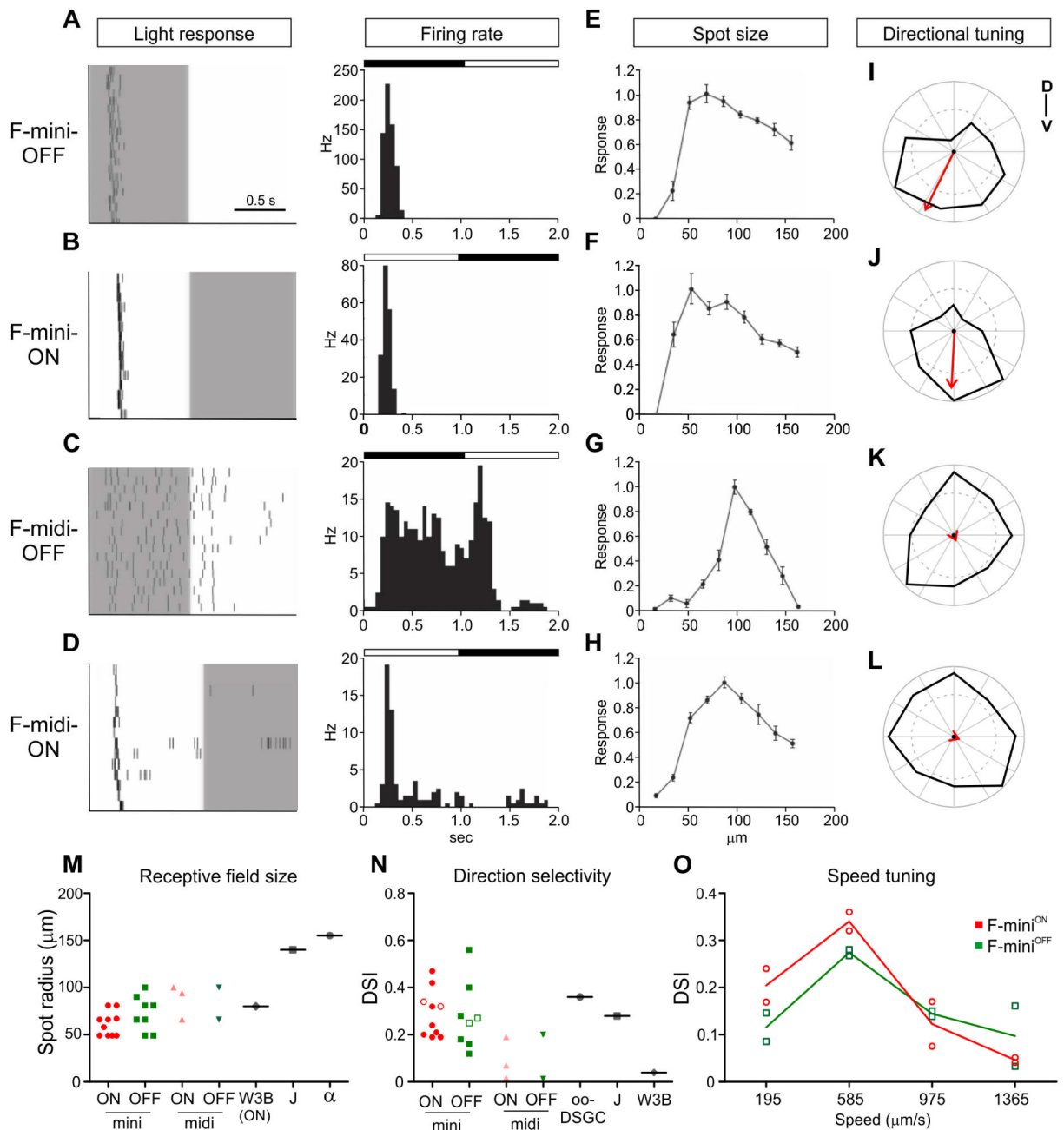
Figure 5. Visual responses of F-RGCs

(A–D) Representative responses to a spot flashing ON (white) and OFF (grey) over the receptive field center for each cell. Raster plots of spikes from 14–20 repeats. Histograms (right) show frequency of spikes over time.

(E–H) Responses to flashing spots of different radii. The number of spikes are plotted during the optimal response period (ON or OFF) for each type, normalized to the maximum response. Each plot shows a single cell and data points averaged across 10 trials for each spot radius (mean ± SE).

(I–L) Responses to bars moving across the receptive field center in different directions. Polar plots represent the number of spikes fired for bars moving in each of the eight directions.

(M) Receptive field size calculated as the optimal spot radius.

(N) Direction selectivity index (DSI) was calculated as the length of the vector sum in the preferred direction divided by the sum of responses to all directions. F-mini RGCs show directional tuning (DSI > 0.25), whereas F-midi cells are direction non-selective (DSI < 0.1). An alternate method for calculating DSI, preferred minus null response, gives DSI of >0.4 for F-mini and <0.2 for F-midi RGCs. n = 10, 8, 3, and 2 cells for F-mini[ON], F-mini[OFF], F-midi[ON], and F-midi[OFF] types. Open circles or squares indicate cells tested for direction selectivity at different speeds. Comparison to other RGC types from Kim et al., 2008, 2010.

(O) Speed tuning curves for F-mini RGCs.

See also Figure S5.
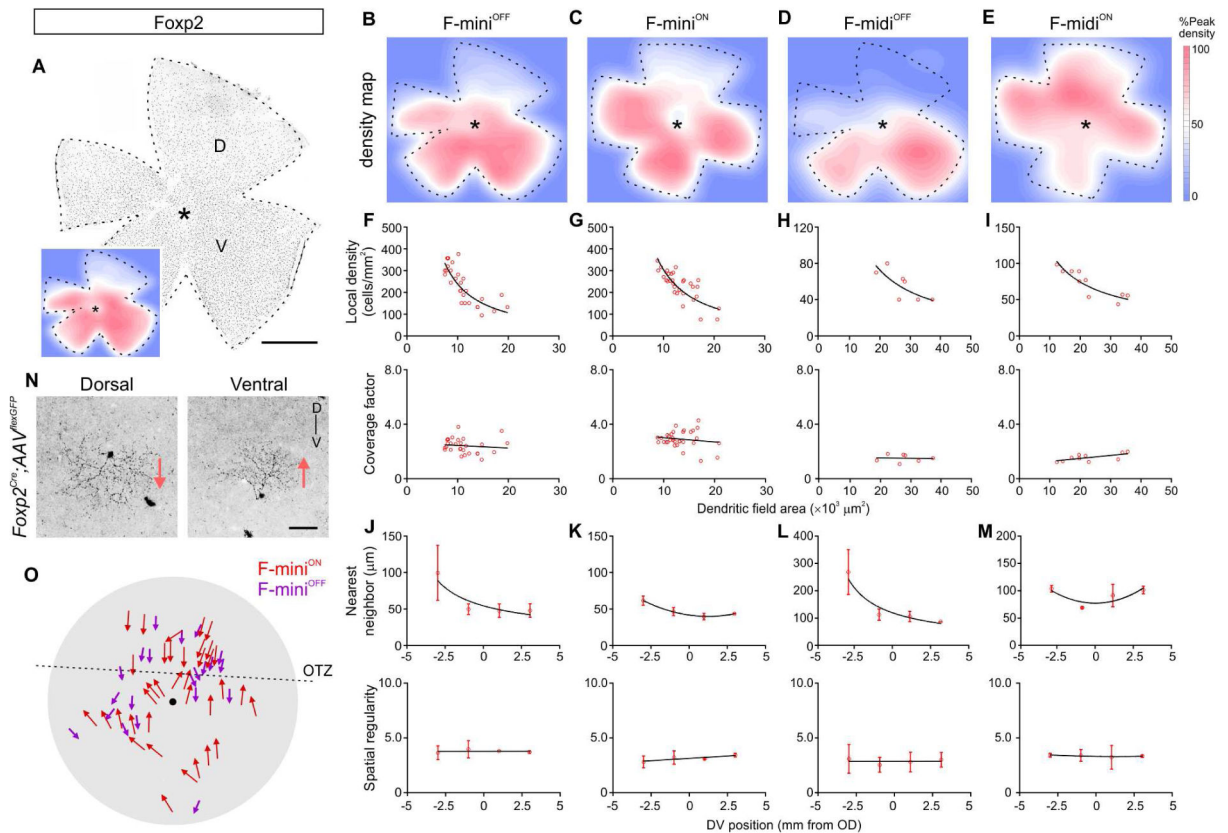
Figure 6. F-RGCs are organized anisotropically along the DV-axis of the retina

(A–E) Whole mount of retina stained for Foxp2 (A). Density heat maps for all F-RGCs (inset in A) and each F-RGC type (B–E) from retinas stained with Foxp2 plus Foxp1 and Brn3 isoforms. D, dorsal; V, ventral; asterisks, optic disk.

(F–I) Scatter plots of dendritic field area versus local density and coverage factor. Density and area co-vary while dendritic coverage stays relatively constant (CF = 2.41 ± 0.10, F-mini^{OFF}; 2.90 ± 0.11, F-mini^{ON}; 1.49 ± 0.10, F-midi^{OFF}; 1.54 ± 0.08, F-midi^{ON}; mean ± SE).

(J–M) Spatial analysis (nearest-neighbor distance and spatial regularity) at different axial positions shows that mosaic spacing is globally maintained for each F-RGC type despite local changes in density.

(N) GFP-labeled F-mini^{ON} RGCs from dorsal and ventral retina.

(O) Position and dendritic orientation of F-mini^{ON} (red) and F-mini^{OFF} (purple) RGCs. All F-mini^{OFF} RGCs point ventrally whereas F-mini^{ON} RGCs point to the opsin transition zone (OTZ; localized as shown in Figure S6C). The dendritic orientation of F-mini^{ON} RGCs located in the ventral retina are inverted with respect to mini^{ON} RGCs located in the dorsal retina. In contrast, F-mini^{OFF} RGCs maintain ventral orientation independent of retinal position.

N = 30, 29, 12, and 7 cells for F-mini^{ON}, F-mini^{OFF}, F-midi^{ON}, and F-midi^{OFF} types, respectively. Scale bar in (A) = 1 mm; (N) = 50 μm. See also Figure S6.
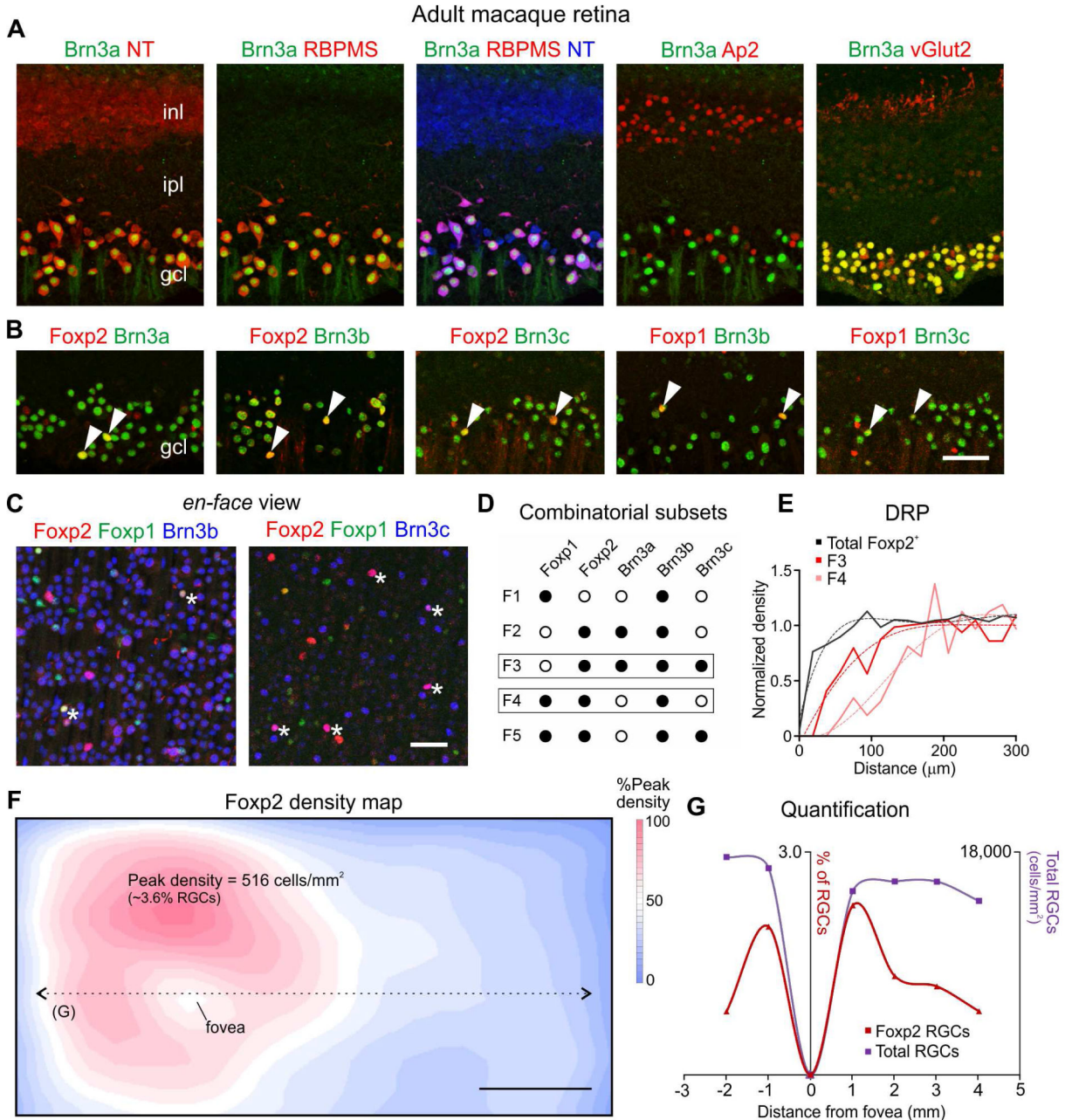
Figure 7. Foxp and Brn3 proteins distinguish RGC types in primate retina

(A, B) Immunostaining analysis of Foxp2, Foxp1, and Brn3 proteins in adult macaque retina. Brn3a is selectively expressed by RGCs localized to the ganglion cell layer (A). Double-staining for Foxp and Brn3 shows their co-localization within subsets (B). Arrows indicate double-positive cells. Neurotrace (NT) was used to label all somata.

(C) Whole mount retinas stained for Foxp1, Foxp2, and Brn3b or Brn3c proteins. Foxp1 and Foxp2 combinatorially distinguish three RGC groups (Foxp1$^+$/Foxp2$^-$, Foxp1$^+$/Foxp2$^+$, and Foxp2$^+$/Foxp1$^-$). Brn3b is co-expressed by the Foxp1$^+$/Foxp2$^+$ group (asterisks in left

panel). Brn3c is co-expressed by a subset of the Foxp2$^+$/Foxp1$^-$ group (asterisks in right panel).

(D) Table summarizing five molecularly distinct RGC types marked by Foxp and Brn3 proteins, provisionally called F1-5.

(E) DRP analysis of total Foxp2$^+$ RGCs suggests that they are a mixture of RGC types. DRP of F3 (red) and F4 (pink) RGCs reveals their non-random mosaic organization, indicating they are a single RGC type.

(F) Density map of Foxp2 RGCs, showing their enrichment around the fovea.

(G) Quantification of total Brn3a$^+$ RGCs and the fraction that are Foxp2$^+$ at different distances from the fovea. Foxp2 RGC density drops by more than half while overall RGC density remains stable. Images and plots are representative from n = 2 retinas. Scale bars in (A–C) = 50 μm; (F) = 1 mm. See also Figure S7.

Table 1

Molecular and genetic labeling of F-RGC types

		F-mini^{ON}	F-midi^{ON}	F-mini^{OFF}	F-midi^{OFF}	others
Transcription factors	Brn3a	+	+	+	+	+
	Brn3b	+	+	–	+	+
	Brn3c	–	+	–	–	+
	Ebf3	–	+	–	–	+
	Foxp1	–	–	+	+	–
	Foxp2	+	+	+	+	–
	Isl1	–	–	+d	+d	+
	Isl2	+	+	+	+	+
	NeuN	+	+	+	+	+
	Satb1	–	+d	–	–	+
	Satb2	–	+d	–	–	+
	Tbr2	–	–	–	–	+
Cytosolic/Membrane proteins	Calbindin	–	–	–	–	+
	Calretinin	+	+	+	+	+
	Parvalbumin	–	–	+d	+d	+
	Calsenilin	+	–	+	–	+
	Cart	–	–	–	–	+
	Kv4.2	+	–	+	–	+
	Melanopsin	–	–	–	–	+
	Ppp1r17	+d	–	–	–	+
	Osteopontin	–	–	–	–	+
Mouse lines	Cdh3-GFP	–	–	–	–	+
	Cdh4-CreER	+	+	+	+	+
	Cdh6-CreER	–	–	–	–	+
	Cdh13-CreER	+	–	+	–	+
	Hb9GFP	–	–	–	–	+
	JamB-CreER	–	–	–	–	+
	PV-Cre	–	–	+	+	+

	F-mini[ON]	F-midi[ON]	F-mini[OFF]	F-midi[OFF]	others
Thwga3	+d	–	–	–	+
Thwga7	–	–	–	–	+

+d, indicates dim staining

See also Figure S4